

# High-Density Phenomena in Hydrogen Plasma<sup>1</sup>

V. S. Filinov\*, M. Bonitz\*\*, and V. E. Fortov\*\*\*

\* Mercator guest professor at Rostock University

\*\* Fachbereich Physik, Universität Rostock, D-18051 Rostock, Germany

\*\*\* High Energy Density Research Center, Joint Institute for High Temperatures, Russian Academy of Sciences, Izhorskaya ul. 13/19, Moscow, 127412 Russia

Received June 27, 2000; in final form, August 1, 2000

A novel path-integral representation of the many-particle density operator is presented which makes direct Fermionic path-integral Monte Carlo simulations feasible over a wide range of parameters. The method is applied to compute the pressure, energy, and pair distribution functions of a hydrogen plasma in the region of strong coupling and strong degeneracy. Our numerical results allow one to analyze the atom and molecule formation and breakup and predict, at high density, proton ordering and pairing of electrons. © 2000 MAIK “Nauka/Interperiodica”.

PACS numbers: 52.25.Kn; 52.65.Pp

Coulomb systems continue to attract the interest of researchers in many fields, including plasmas, astrophysics and solids; see [1, 2] for an overview. The most interesting phenomena, such as metallic hydrogen, plasma phase transition, bound states, etc., occur in situations where the plasma is both strongly coupled and strongly degenerate. However, in this region, the thermodynamic properties of the plasma are only poorly known. The need for the simultaneous account of strong Coulomb and quantum effects makes a theoretical treatment very difficult. Among the most promising theoretical approaches to these systems are path-integral quantum Monte Carlo (PIMC) techniques; see, e.g., [3, 4].

In this letter, we demonstrate that for many current problems in dense warm plasmas ( $k_B T > 0.1$  Ry), direct PIMC simulations can, in fact, be carried out with acceptable efficiency. We report results for the internal energy, equation of state, and pair distribution functions of partially ionized hydrogen in a wide range of coupling and degeneracy parameters,  $\Gamma = (4\pi n_e/3)^{1/3} e^2/4\pi\epsilon_0 k_B T$  and  $\chi = n_e \lambda_e^3$  ( $\lambda_e$  is the electron thermal wave length  $\lambda_e^2 = 2\pi\hbar^2\beta/m_e$ ). Furthermore, our calculations predict ordering of protons, as well as pairing of electrons, at high density.

As is well known, the thermodynamic properties of a quantum system are fully determined by the partition function  $Z$ . For a binary mixture of  $N_e$  electrons and  $N_i$

protons,  $Z$  is conveniently written as

$$Z(N_e, N_i, V, \beta) = Q(N_e, N_i, \beta)/N_e!N_i!,$$

$$Q(N_e, N_i, \beta) = \sum_{\sigma} \int d\mathbf{q} d\mathbf{r} \rho(\mathbf{q}, \mathbf{r}, \sigma; \beta). \quad (1)$$

Here,  $\mathbf{q} \equiv \{\mathbf{q}_1, \mathbf{q}_2, \dots, \mathbf{q}_{N_i}\}$  comprises the coordinates of the protons and  $\sigma = \{\sigma_1, \dots, \sigma_{N_e}\}$  and  $\mathbf{r} \equiv \{\mathbf{r}_1, \dots, \mathbf{r}_{N_e}\}$  are the electron spins and coordinates, respectively. The density matrix  $\rho$  in Eq. (1) is represented in the standard way by a path integral [5]:

$$\rho(\mathbf{q}, \mathbf{r}, \sigma; \beta) = \frac{1}{\lambda_i^{3N_i} \lambda_\Delta^{3N_e}} \sum_P (\pm 1)^{\kappa_P} \int_V d\mathbf{r}^{(1)} \dots d\mathbf{r}^{(n)} \quad (2)$$

$$\times \rho(\mathbf{q}, \mathbf{r}, \mathbf{r}^{(1)}; \Delta\beta) \dots \rho(\mathbf{q}, \mathbf{r}^{(n)}, \hat{P}\mathbf{r}^{(n+1)}; \Delta\beta) \mathcal{S}(\sigma, \hat{P}\sigma),$$

where  $\Delta\beta \equiv \beta/(n+1)$  and  $\lambda_\Delta^2 = 2\pi\hbar^2\Delta\beta/m_e$ . Further,  $\mathbf{r}^{(n+1)} \equiv \mathbf{r}$  and  $\sigma' = \sigma$ ; i.e., the particles are represented by fermionic loops with the coordinates (beads)  $[\mathbf{r}] \equiv [\mathbf{r}, \mathbf{r}^{(1)}, \dots, \mathbf{r}^{(n)}, \mathbf{r}]$ . The electron spin gives rise to the spin part of the density matrix  $\mathcal{S}$ , whereas exchange effects are accounted for by the permutation operator  $\hat{P}$  and the sum over the permutations with parity  $\kappa_P$ . Following [3, 6, 7], we use a modified representation (3) of the high-temperature density matrices on the r.h.s. of Eq. (2), which is suitable for efficient direct fermionic PIMC simulations of plasmas. With the error of order  $\epsilon \sim (\beta Ry)^2 \chi/(n+1)$  vanishing with a growing number of beads, we obtain the approximation

$$\sum_{\sigma} \rho(\mathbf{q}, \mathbf{r}, \sigma; \beta) = \frac{1}{\lambda_i^{3N_i} \lambda_\Delta^{3N_e}} \sum_{s=0}^{N_e} \rho_s(\mathbf{q}, [\mathbf{r}], \beta),$$

<sup>1</sup> This article was submitted by the authors in English.

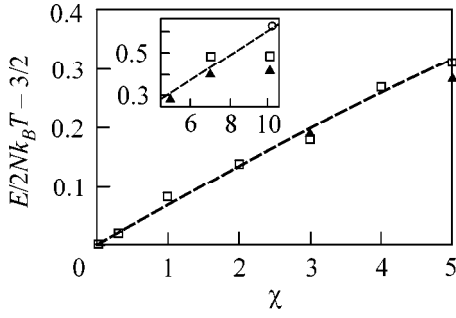


**Fig. 1.** Energy  $E$  of an ideal plasma of degenerate electrons and classical protons in excess of the classical energy. PIMC simulation results with varied particle number are shown:  $N = 32$  (triangles),  $N = 50$  (squares), and  $N = 90$  (circles) are compared to the exact analytical result (dashed line).

$$\rho_s(q, [r], \beta) = \frac{C_{N_e}^s}{2^{N_e}} \exp\{-\beta U(q, [r], \beta)\} \times \prod_{l=1}^n \prod_{p=1}^{N_e} \phi_{pp}^l \det|\Psi_{ab}^{n,1}|_s, \quad (3)$$

$$U(q, [r], \beta) = U^i(q) + \sum_{l=0}^n \frac{U_l^e([r], \beta) + U_l^{ei}(q, [r], \beta)}{n+1},$$

where  $U^i$ ,  $U_l^e$ , and  $U_l^{ei}$  denote the sum of the binary interaction Kelbg potentials  $\Phi^{ab}$  [8] between protons, electrons at vertex  $l$ , and electrons (vertex  $l$ ) and protons, respectively.

In Eq. (3),  $\phi_{pp}^l \equiv \exp[-\pi|\xi_p^{(l)}|^2]$  arises from the kinetic energy density matrix of the electron with index  $p$ , and we introduced dimensionless distances between neighboring vertices on the loop,  $\xi^{(1)}, \dots, \xi^{(n)}$ . Thus, explicitly,  $[r] \equiv [r; r + \lambda_\Delta \xi^{(1)}; r + \lambda_\Delta(\xi^{(1)} + \xi^{(2)}); \dots]$ . The exchange matrix is given by

$$\|\Psi_{ab}^{n,1}\|_s \equiv \left\| \exp\left\{-\frac{\pi}{\lambda_\Delta^2} |(r_a - r_b) + y_a^n|^2\right\} \right\|_s, \quad (4)$$

$$y_a^n = \lambda_\Delta \sum_{k=1}^n \xi_a^{(k)}.$$

As a result of the spin summation, the matrix carries a subscript  $s$  denoting the number of electrons having the same spin projection.

As an example, we present the equation of state  $\beta p = \partial \ln Q / \partial V = [\alpha / 3V \partial \ln Q / \partial \alpha]_{\alpha=1}$ :

$$\frac{\beta p V}{N_e + N_i} = 1 + \frac{(3Q)^{-1}}{N_e + N_i} \sum_{s=0}^{N_e} \int dq dr d\xi \rho_s(q, [r], \beta)$$

$$\times \left\{ \sum_{p < t}^{N_i} \frac{\beta e^2}{|q_{pt}|} - \sum_{p < t}^{N_e} |r_{pt}| \frac{\partial \Delta \beta \Phi^{ee}}{\partial |r_{pt}|} - \sum_{p=1}^{N_i} \sum_{t=1}^{N_e} |x_{pt}| \frac{\partial \Delta \beta \Phi^{ie}}{\partial |x_{pt}|} - \sum_{l=1}^n \left[ \sum_{p < t}^{N_e} A_{pt}^l \frac{\partial \Delta \beta \Phi^{ee}}{\partial |r_{pt}^l|} + \sum_{p=1}^{N_i} \sum_{t=1}^{N_e} B_{pt}^l \frac{\partial \Delta \beta \Phi^{ie}}{\partial |x_{pt}^l|} \right] + \frac{\alpha}{\det|\Psi_{ab}^{n,1}|_s} \frac{\partial \det|\Psi_{ab}^{n,1}|_s}{\partial \alpha} \right\}, \quad (5)$$

$$A_{pt}^l = \frac{\langle r_{pt}^l | r_{pt}^l \rangle}{|r_{pt}^l|}, \quad B_{pt}^l = \frac{\langle x_{pt}^l | x_{pt}^l \rangle}{|x_{pt}^l|}.$$

Here,  $\alpha$  is a length scaling;  $\alpha = L/L_0$ ,  $\langle \dots | \dots \rangle$  denotes the scalar product; and  $q_{pt}$ ,  $r_{pt}$ , and  $x_{pt}$  are the differences of two coordinate vectors:  $q_{pt} \equiv q_p - q_t$ ,  $r_{pt} \equiv r_p - r_t$ ,  $x_{pt} \equiv r_p - q_t$ ,  $r_{pt}^l \equiv r_{pt} + y_{pt}^l$ ,  $x_{pt}^l \equiv x_{pt} + y_{pt}^l$ ,  $y_{pt}^l = \lambda_\Delta \sum_{k=1}^n \xi_p^{(k)}$ , and  $y_{pt}^l \equiv y_p^l - y_t^l$ . Other thermodynamic quantities have an analogous form.

We demonstrate our numerical scheme for a two-component electron–proton plasma. In the simulations, we used  $N_e = N_p = 50$ . To test the MC procedure, we first consider a mixture of ideal electrons and protons for which the thermodynamic quantities are known analytically, e.g., [9]. Figure 1 shows our numerical results for the pressure, together with the theoretical curve. The agreement, up to the degeneracy parameter  $\chi$  as large as 10, is evident and improves with increasing particle number. This clearly proves that our method correctly samples the fermionic permutations. Note that for fast generation of a MC sequence of  $N$ -particle configurations it is necessary to efficiently compute the acceptance probability of new configurations, which is proportional to the absolute value of the ratio of the exchange determinants of two subsequent configurations, while the sign of the determinants is included in the weight function of each configuration.

Let us now turn to the case of interacting electrons and protons. We performed a series of calculations in which the classical coupling parameter  $\Gamma$  was kept constant while the degeneracy parameter  $\chi$  was varied, cf. Fig. 2. One can see that, for weak coupling ( $\Gamma = 0.4$ ) and small degeneracy parameters  $\chi < 0.5$ , there is good agreement with analytical theories and quantum MC simulations without exchange [10]. However, as expected, with increasing  $\chi$  and  $\Gamma$ , the deviations grow rapidly. Figure 2 also contains a comparison with restricted path-integral results of Militzer *et al.* [11] (the large triangles) corresponding to values of the coupling parameter in the range of 0.17,  $\dots$ , 0.672. Evidently, the agreement, in particular, of the energies, is very good. The deviations in the pressure are apparently related to the fixed-node approximation used in [11] and need further investigation.

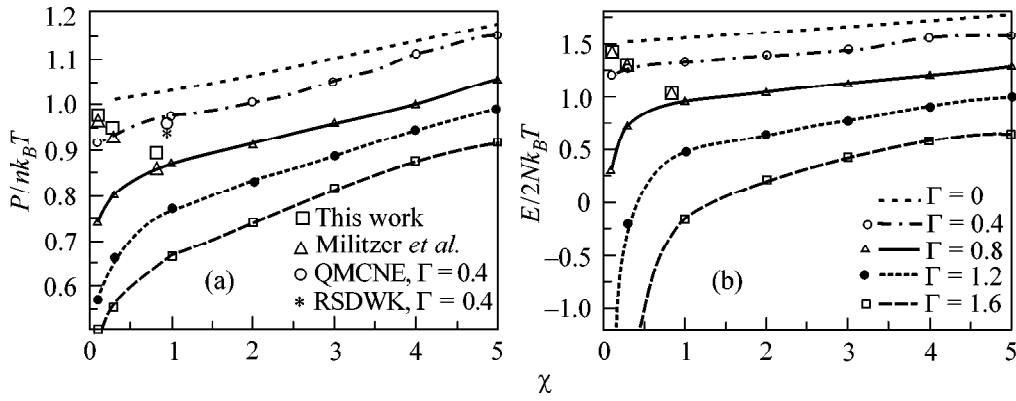


**Fig. 2.** (a) Pressure  $P$  and (b) energy  $E$  of the *nonideal* plasma as functions of the quantum parameter  $\chi$ . Curves correspond to different values of the coupling parameter  $\Gamma$  given in the inset of the right figure. Large circle denotes quantum MC simulations without exchange (QMCNE), and large asterisk denotes the weak coupling model of Riemann *et al.* (RSDWK), using data from [10]. The large triangles are recent restricted PIMC results of Militzer *et al.* [11], which are compared to our results (large squares) for three values of  $\Gamma$ , from top to bottom:  $\Gamma = 0.169, 0.338$ , and  $0.672$ .

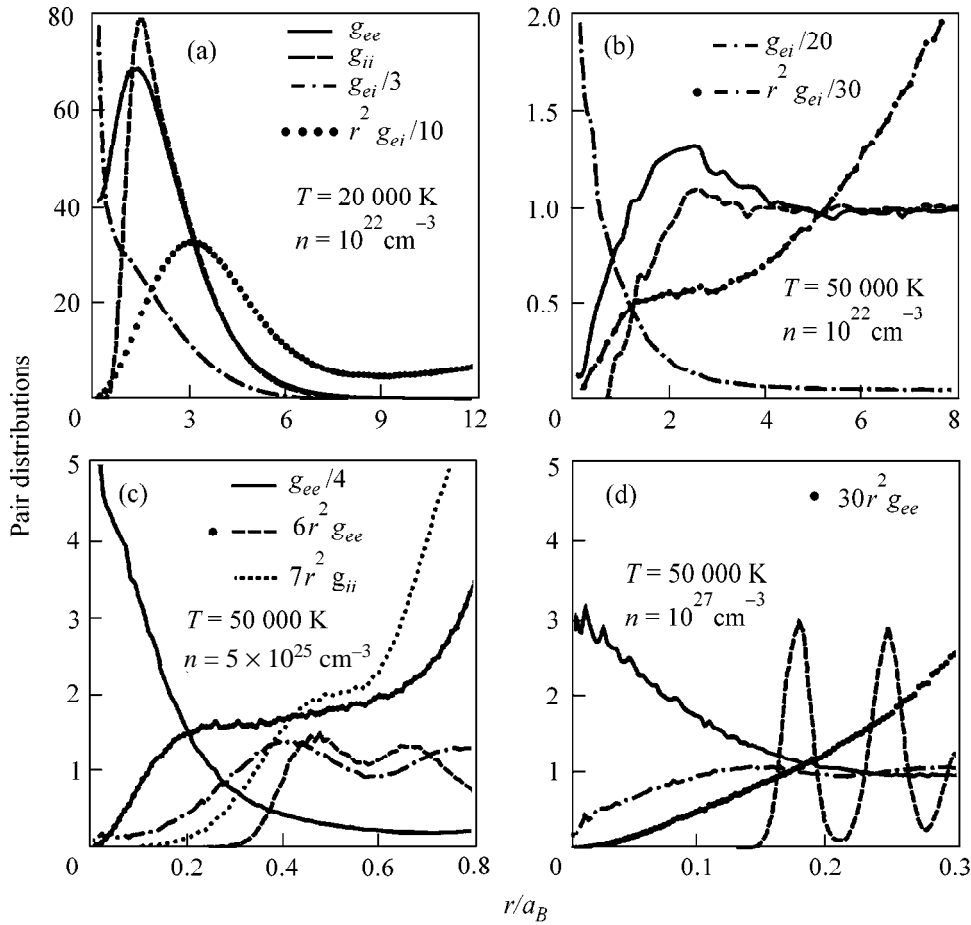


**Fig. 3.** Electron–electron ( $g_{ee}$ , full line), ion–ion ( $g_{ii}$ , dashed line) and electron–ion ( $g_{ei}$ , dash–dotted line) pair distribution functions for dense hydrogen. The line styles in (b) and (c) are the same as in (a). Notice the varying scalings of the curves. The values for the coupling, degeneracy, and Brueckner parameters are (a)  $\Gamma = 2.9, \chi = 1.46, r_s = 5.44$ ; (b)  $\Gamma = 1.16, \chi = 0.37, r_s = 5.44$ ; (c)  $\Gamma = 19.8, \chi = 1848, r_s = 0.318$ ; and (d)  $\Gamma = 53.8, \chi = 37.000, r_s = 0.117$ .

A very interesting result is that the energy curves in Fig. 2 become almost parallel as the degeneracy increases. In contrast, for  $\Gamma > 0.6$ , reduction of  $\chi$  leads to a rapid decrease in the energy, which is due to the

formation of atoms and molecules, as will be shown below.

The main advantage of the presented method is that it allows one to investigate dense plasmas in a variety

of physical situations which are very difficult to describe reliably by other approaches. This includes partial ionization and dissociation, Mott effect, and ionic ordering at high densities. To investigate these phenomena, we show, in Fig. 3, the pair distribution functions for the four most interesting physical situations. Figure 3a clearly shows the existence of hydrogen molecules (cf. the peaks of the proton–proton and electron–electron pair distribution functions at a separation of about  $1.4a_B$ ) and atoms. We note that the peak of the electron–proton function (multiplied by  $r^2$ ) in our calculations appears at  $r = 1a_B$  if no molecules are present (e.g., at lower density). But for the situation of Fig. 3a, the presence of molecules leads to a shift of the peak to larger distances. Figure 3b shows that, with increasing temperature, atoms and molecules break up, which is clearly seen by the drastic lowering of the mentioned peaks in the pair distribution functions.

Let us now consider the case of higher densities, but keep the temperature constant. Here, our calculations predict interesting physical phenomena. In Figs. 3b–3d, one clearly sees increased ordering of protons from a partially ionized plasma (3b,  $\Gamma \approx 1.2$ ), to liquidlike (3c,  $\Gamma \approx 20$ ) and solidlike (3d,  $\Gamma \approx 54$ ) behavior, cf. the proton–proton pair distribution functions.

Notice further a qualitative change in the electron–electron function upon a density increase from Fig. 3b to 3d:  $g_{ee}$  in Fig. 3b is typical of partially ionized plasmas, whereas in Fig. 3c a strong peak at small distances is observed. A further increase in the density leads to an almost uniform electron distribution in Fig. 3d. For better understanding of the electron behavior, we also included in Fig. 3c the functions  $r^2g_{ee}$  and  $r^2g_{ii}$ . The shoulders in these curves indicate that the most probable interelectronic distance is almost two times smaller than the average distance between two protons. The reason for the behavior in Fig. 3c is *pairing of electrons* with opposite spin projections. An analysis of the electronic bead distribution allows us to conclude that the “extension” of the electrons is of the order of the interion distance and that there is partial overlap of individual electrons. Under these conditions, pairing of (part of) the electrons minimizes the total energy of the system. This effect vanishes with increasing density due to the growing wave function overlap.

This work was supported by the Deutsche Forschungsgemeinschaft (Mercator-Programm) and the NIC Jülich. We acknowledge stimulating discussions with W. Ebeling, D. Kremp, W.D. Kraeft, and M. Schlanges and thank B. Militzer for providing the data of [11].

## REFERENCES

1. H. E. DeWitt *et al.*, W. Ebeling *et al.*, and D. Klakow *et al.*, in *Proceedings of the International Conference on Strongly Coupled Plasmas*, Ed. by W. D. Kraeft and M. Schlanges (World Scientific, Singapore, 1996).
2. J. Shumway and D. M. Ceperley, in *Proceedings of the International Conference on Strongly Coupled Coulomb Systems, Saint-Malo, France, 1999*; *J. Phys. IV* **10** (5), 3 (2000); J. P. Hansen, D. Goulding, and R. van Roij, in *Proceedings of the International Conference on Strongly Coupled Coulomb Systems, Saint-Malo, France, 1999*; *J. Phys. IV* **10** (5), 27 (2000); M. Rosenberg, in *Proceedings of the International Conference on Strongly Coupled Coulomb Systems, Saint-Malo, France, 1999*; *J. Phys. IV* **10** (5), 73 (2000).
3. V. M. Zamalin, G. E. Norman, and V. S. Filinov, *The Monte Carlo Method in Statistical Thermodynamics* (Nauka, Moscow, 1977).
4. D. Ceperley, *The Monte Carlo and Molecular Dynamics of Condensed Matter Systems*, Ed. by K. Binder and G. Cicotti (SIF, Bologna, 1996).
5. R. P. Feynman and A. R. Hibbs, *Quantum Mechanics and Path Integrals* (McGraw-Hill, New York, 1965).
6. V. S. Filinov, *High Temp.* **13**, 1065 (1975); **14**, 225 (1976).
7. B. V. Zelener, G. E. Norman, and V. S. Filinov, *High Temp.* **13**, 650 (1975).
8. G. Kelbg, *Ann. Phys. (Leipzig)* **12**, 219 (1963); **13**, 354 (1963); **14**, 394 (1964); W. Ebeling, H. J. Hoffmann, and G. Kelbg, *Beitr. Plasmaphys.* **7**, 233 (1967) and references therein.
9. W. D. Kraeft, D. Kremp, W. Ebeling, and G. Röpke, *Quantum Statistics of Charged Particle Systems* (Akademie, Berlin, 1986; Mir, Moscow, 1988).
10. J. Riemann, M. Schlanges, H. E. DeWitt, and W. D. Kraeft, in *Proceedings of the International Conference on Strongly Coupled Plasmas*, Ed. by W. D. Kraeft and M. Schlanges (World Scientific, Singapore, 1996), p. 82.
11. B. Militzer and D. Ceperley, submitted to *Phys. Rev. Lett.*